NOAA Technical Memorandum OAR PMEL-142

CURVILINEAR VERSION OF THE MOST MODEL WITH APPLICATION TO THE COAST-WIDE TSUNAMI FORECAST

David Burwell[1,2]
Elena Tolkova[1,2]

[1]Joint Institute for the Study of the Atmosphere and Ocean (JISAO)
University of Washington, Seattle, WA

[2]Pacific Marine Environmental Laboratory
Seattle, WA

Pacific Marine Environmental Laboratory
Seattle, WA
August 2008

UNITED STATES DEPARTMENT OF COMMERCE

Carlos M. Gutierrez
Secretary

NATIONAL OCEANIC AND ATMOSPHERIC ADMINISTRATION

VADM Conrad C. Lautenbacher, Jr.
Under Secretary for Oceans and Atmosphere/Administrator

Office of Oceanic and Atmospheric Research

Richard W. Spinrad
Assistant Administrator

NOTICE from NOAA

Mention of a commercial company or product does not constitute an endorsement by NOAA/OAR. Use of information from this publication concerning proprietary products or the tests of such products for publicity or advertising purposes is not authorized. Any opinions, findings, and conclusions or recommendations expressed in this material are those of the authors and do not necessarily reflect the views of the National Oceanic and Atmospheric Administration.

Contribution No. 3231 from NOAA/Pacific Marine Environmental Laboratory

Also available from the National Technical Information Service (NTIS)
(`http://www.ntis.gov`)

Contents

List of Figures

Curvilinear version of the MOST model with application to the coast-wide tsunami forecast

D. Burwell[1,2] and E. Tolkova[1,2]

Abstract. The tsunami forecasting system being developed at the NOAA Center for Tsunami Research (NCTR) employs the Method Of Splitting Tsunami (MOST) numerical model in order both to compute ocean-wide tsunami propagation scenarios and to zoom in on a tsunami wave within a limited near-shore area. The present two-part publication describes a particular set-up of the model used for coast-wide tsunami wave height estimation, the Regional Forecast. The publication also describes a version of the MOST model that allows data fields to be sampled on arbitrary orthogonal curvilinear grids. With the curvilinear version of the model, the Regional Forecast can be used with shoreline-following grids, which is more efficient computationally and can result in a more accurate estimate.

Part I presents the ideas behind the Regional Forecast and its verification with higher-resolution models.

Part II introduces a curvilinear version of the MOST model. Particular attention is given to

- developing the governing equations in an arbitrary orthogonal curvilinear coordinate system;
- the course of the MOST code development, of which the present work is a part;
- the modifications in the code due to grids' curvilinearity;
- the technique of developing the shoreline-oriented grids;
- the features of the next version of the Regional Forecast.

[1]Joint Institute for the Study of the Atmosphere and Ocean, University of Washington, Seattle, WA

[2]NOAA, Pacific Marine Environmental Laboratory, Seattle, WA

Part I: Regional Forecast Version 1

(Burwell and Tolkova)

1. Ideas behind the Regional Forecast

The current version of the tsunami forecast system being developed in the NOAA Center for Tsunami Research (NCTR) is based on site-specific Stand-by Inundation Models (SIMs) (Titov *et al.*, 2005). SIMs are implementations of the Method Of Splitting Tsunami (MOST) numerical algorithm (Titov and Synolakis, 1998) with three telescopic grids with a typical resolution of about 2–4 sec of arc (grid C), 9–24 sec (grid B), 1–2 min (grid A), adjusted to specific locations and tested against a wide range of tsunami scenarios at these locations (Titov and González, 1997; Tang *et al.*, 2006). As shown by historical data and recent events, SIMs provide fairly good agreement between time series calculated at the point of a tide gage location in the inner grid (C) and the actual data recorded at the gage (Wei *et al.*, 2008). Overall, SIMs provide a detailed picture of tsunami wave behavior in the relatively small area enclosed in grid C.

Complementary to SIMs, the Regional Forecast tool was developed to evaluate the tsunami hazard for the whole U.S. coastline, not just for selected sites. The tool focuses on estimating the maximum wave height along the coastline, which is assumed to represent the most important parameter for hazard evaluation and warning purposes. Maximum wave height, especially when attributed to a section of the coastline rather than to a point, is not as sensitive to grid resolution as the instant wave height at every time moment at each particular location. Therefore, reliable calculations of near-shore maximum wave height can be performed at a coarser resolution than that of grid C, and without carrying calculations inland, thus not calculating inundation area and not using topography.

This conclusion is based on the following observation: SIMs showed a good agreement between time series in a majority of corresponding points in grid C (high resolution, run-up on land is calculated) and in grid B (lower resolution, calculations are not carried shallower than 1 m of undisturbed water depth). Therefore, grid C may not be needed for the purpose of estimating maximum wave height on the coastline. Also, due to the MOST numerical properties (Burwell *et al.*, 2007), smaller-scale details of a wave shape entering grid B get diffused and dispersed as the wave propagates onshore inside grid B.

Therefore, the wave can be input in grid B at even coarser resolution than that of grid A, without significant loss in the precision of modeled values near

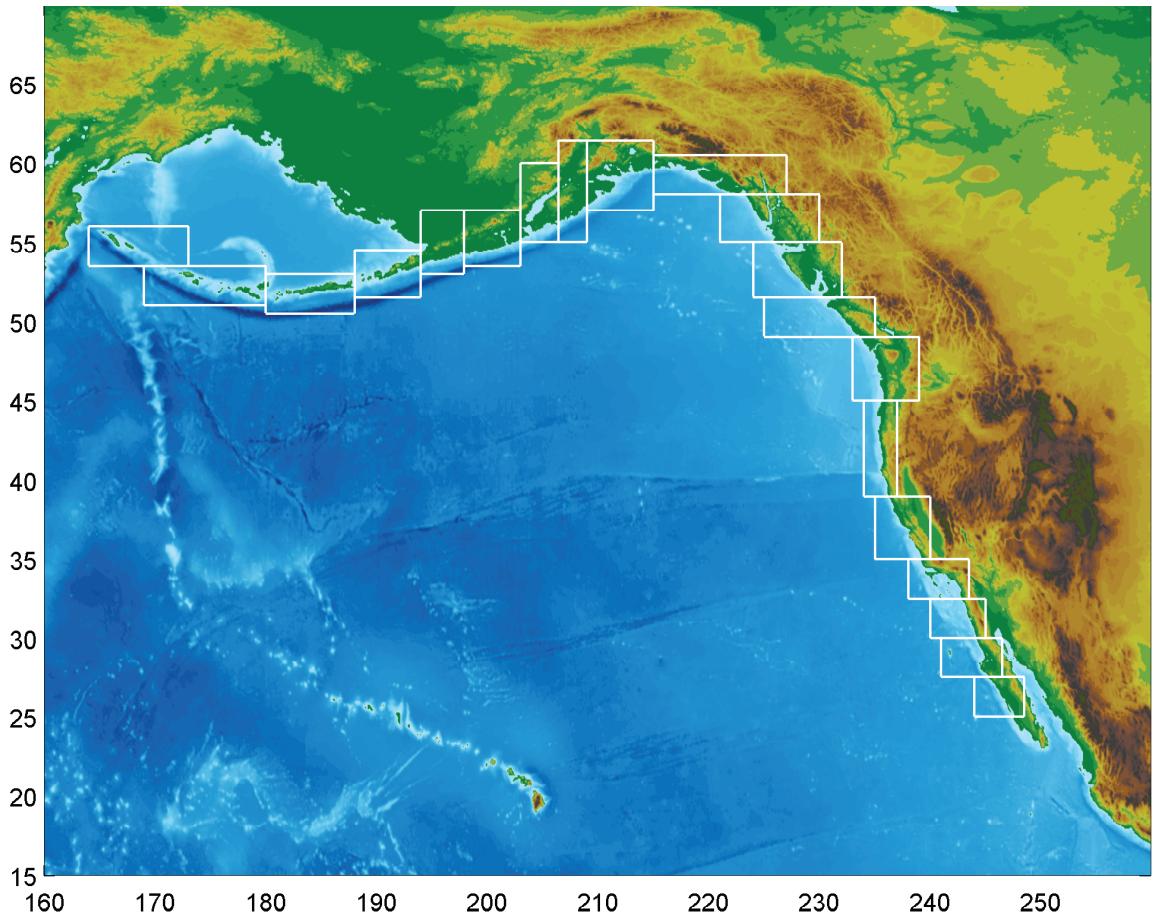

Figure 1-1: Regional Forecast coverage with 20 grids; grids are numbered from west to east. Axes: longitude (°E), latitude (°N).

the shore. Thus for the Regional Forecast purposes, a large enough grid B may receive its input directly from the propagation database.

2. Regional Forecast Implementation and Testing

In its current version, the Regional Forecast for the West Coast and Alaska regions makes use of 20 large grids covering the entire Pacific shoreline of the U.S. (see Fig. 1-1) and can be supplemented by 53 small grids, also covering the same shoreline. Large grids exist at 30-sec, 60-sec, and 120-sec resolution. Small grid resolution is 30 sec.

As part of the Regional Forecast testing, the propagation of a tsunami associated with a 9+ Mw earthquake in the Alaskan-Aleutian subduction zone (unit sources AB 10–14, slip = 30 m) was modeled in all the grids mentioned above. The results obtained with large fine grids (30-sec reso-

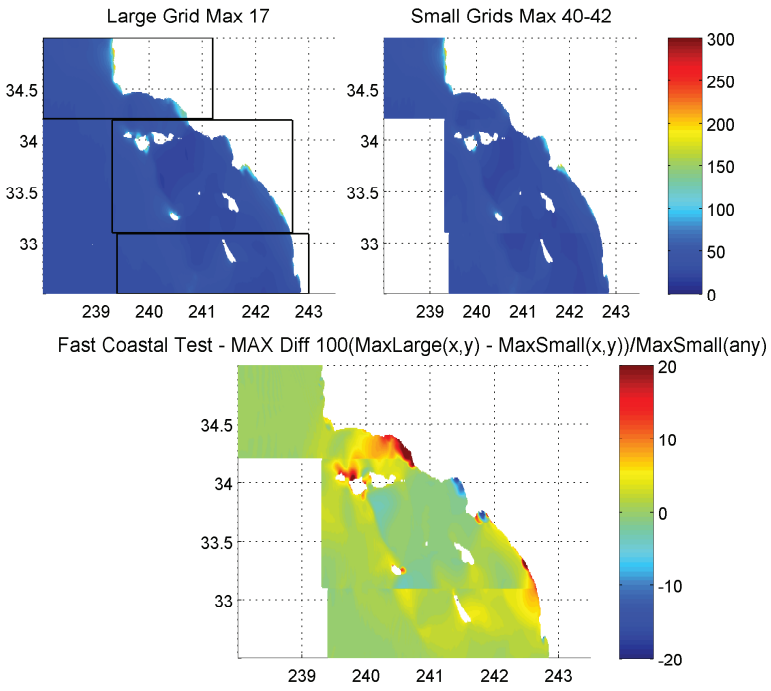

Figure 1-2: Maximum wave height calculated inside a bigger grid (top left, grid 17), inside three smaller ones (grids 40–42) covering the same section of the shoreline (top right), and relative difference in the results (bottom pane). All grids' resolution is 30 sec. Axes: longitude (°E), latitude (°N). Colorbar: cm (top), percent (bottom).

lution) are considered to be the reference. It takes from 20 min to 1 hour of computer time (Dell PowerEdge Linux machine, 2 × 3.6 GHz CPUs) to simulate 10 hours of tsunami propagation using reference grids.

To estimate how coarse or small a grid can be, the difference in maximum wave heights calculated at the same location with a smaller or coarser grid and a corresponding reference grid were introduced. This difference was computed as a percentage of the maximum wave elevation in the entire grid being evaluated. An example of such a comparison is shown in Fig. 1-2 through 1-4.

Figure 1-2 shows the tsunami maximum wave height distribution in reference grid 17 and in smaller grids covering the same section of the shoreline, and the relative difference in these distributions. It takes 5–10 min per grid to perform computations in small grids.

Figure 1-3 shows the tsunami maximum wave height distribution in grid 17 at reference and more coarse (60-sec) resolution, and the relative difference in the results. Computations at 60-sec resolution take 3–7 min per large grid.

Figure 1-4 shows the tsunami maximum wave height distribution in grid 17 at reference and even coarser (120-sec) resolution, and the relative dif-

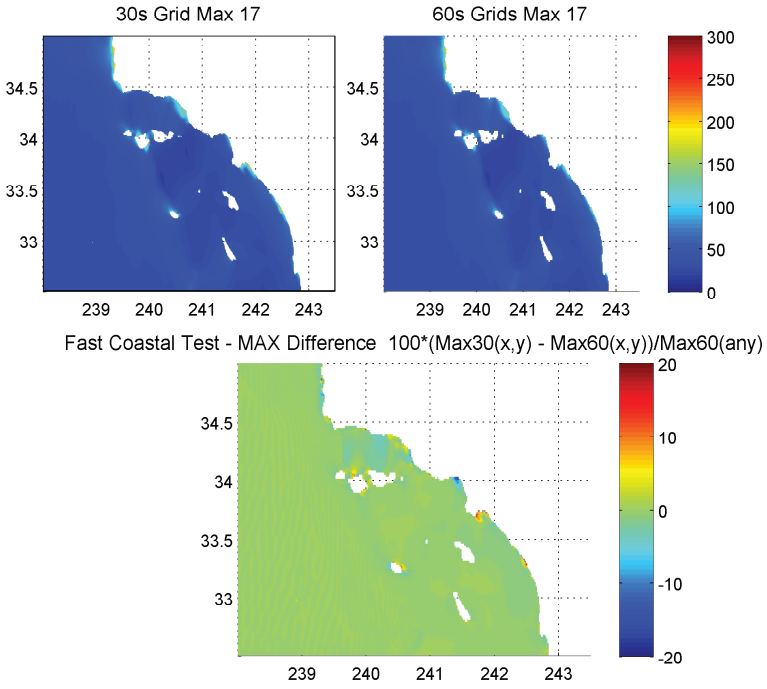

Figure 1-3: Maximum wave height calculated inside a 30-sec resolution grid 17 (top left), inside a 60-sec resolution grid 17 (top right), and relative difference in the results (bottom panel). Axes: longitude (°E), latitude (°N). Colorbar: cm (top), percent (bottom).

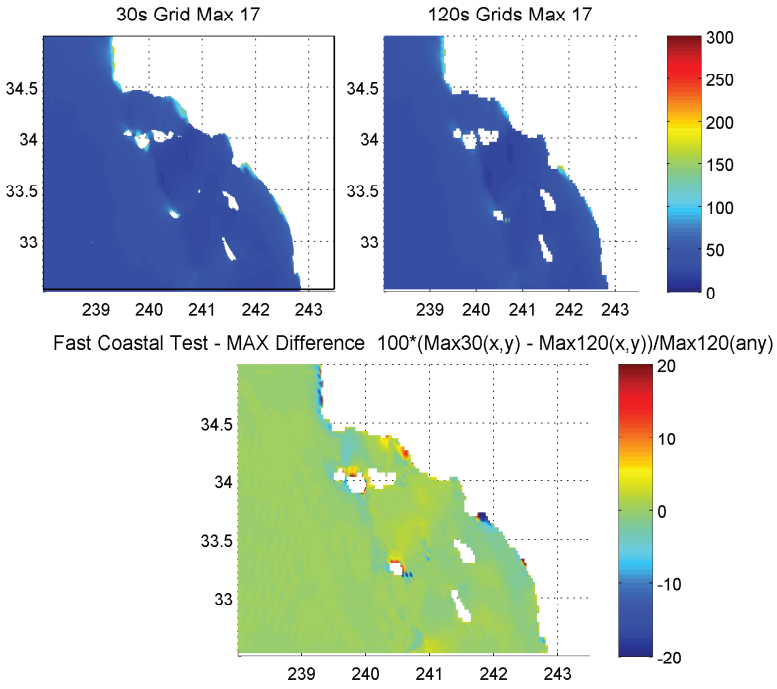

Figure 1-4: Maximum wave height calculated inside a 30-sec resolution grid 17 (top left), inside a 120-sec resolution grid 17 (top right), and relative difference in the results (bottom panel). Axes: longitude (°E), latitude (°N). Colorbar: cm (top), percent (bottom).

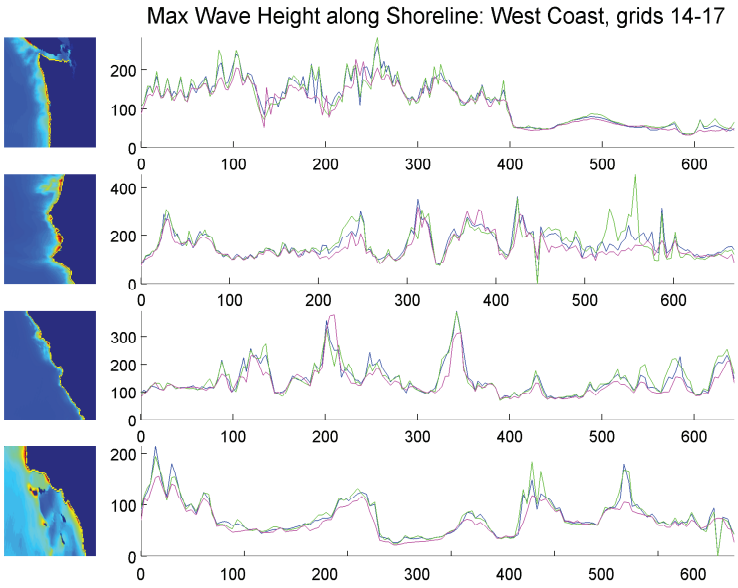

Figure 1-5: Maximum wave height (vertical axes, cm) along coastline (horizontal axes, km) calculated with 30-sec resolution (green), 60-sec (blue) and 120-sec (magenta) in grids 14–17.

ference in the results. A tsunami simulation at 120-sec resolution takes less than 1 min in any large grid.

It can be seen that, whatever the differences in computational expenses (run times) are, all the grids introduced above, regardless of their size or resolution, provide generally the same picture of high and low wave spots. The best agreement with the reference, however, is achieved with a large 60-sec grid, where the relative difference in maximum wave height is under 20% almost everywhere. The same is true for all 20 grids.

The recommended grid set for the Regional Forecast is 60-sec large grids. All the grids receive input from the propagation database and can be run independently. Therefore, using a 20-processor system, tsunami wave heights along the entire Pacific coast of the U.S. can be estimated in a few minutes. Coarser 120-sec grids are faster to run (under 1 min each) and could be used to provide a fast general picture of the locations of high/low amplitude. However, wave height estimate errors would not be under 20% in many coastal areas.

Figure 1-5 is an example of the maximum water elevation along a coastline, calculated at three resolutions. 30-sec and 60-sec resolution values are close to each other, while the picture in 120 sec can be different at some places. The range of values from minimum to maximum of the maximum wave height on a section of the coastline in 60-sec data is suggested as a range of expected wave heights in this area of the coast.

The Regional Forecast is based on MOST version 3, which allows for an arbitrary number and configuration of grids.

Part II: Curvilinear MOST and its First Application: Regional Forecast Version 2

(Tolkova)

1. Curvilinear MOST: The Theory

1.1 The Equations

The numerical model used in the NOAA Center for Tsunami Research (NCTR) for tsunami modeling and forecasting employs the Method Of Splitting Tsunami (MOST) (Titov and Synolakis, 1998) to solve a system of depth-averaged continuity and shallow-water equations:

$$\frac{\partial h}{\partial t} + div\left(h\overrightarrow{V}\right) = 0 \tag{1a}$$

$$\left(\frac{\partial}{\partial t} + \overrightarrow{V}\cdot\bigtriangledown\right)\overrightarrow{V} + g\bigtriangledown h = g\bigtriangledown d \tag{1b}$$

where $h(x_1, x_2, t) = \eta(x_1, x_2, t) + d(x_1, x_2)$, η and d refer to the free surface displacement and undisturbed water depth, respectively, $\overrightarrow{V}(x_1, x_2, t)$ is the depth-averaged velocity vector in the horizontal plane, and g is the acceleration due to gravity.

The MOST model was originally developed in either Cartesian or spherical coordinates (Titov and Synolakis, 1998), based on the method of fractional steps (Yanenko, 1971) and the previously developed one-dimensional tsunami propagation and inundation model with a varying space step (Titov and Synolakis, 1995). Details about the MOST numerical scheme can also be found in Burwell *et al.* (2007). In this work, the MOST numerical realization in an arbitrary orthogonal curvilinear coordinate system is discussed.

Let $x = x(x_1, x_2)$ and $y = y(x_1, x_2)$ be the transition from some orthogonal curvilinear coordinates (x_1, x_2) to the rectangular coordinates (x, y). Then

$$div\left(h\overrightarrow{V}\right) = \frac{1}{\sqrt{\zeta}}\left(\frac{\partial}{\partial x_1}\left(hV_1\sqrt{\zeta_{22}}\right) + \frac{\partial}{\partial x_2}\left(hV_2\sqrt{\zeta_{11}}\right)\right),$$
$$\bigtriangledown = \left(\frac{1}{\sqrt{\zeta_{11}}}\frac{\partial}{\partial x_1},\ \frac{1}{\sqrt{\zeta_{22}}}\frac{\partial}{\partial x_2}\right),$$

where $V_1,\ V_2$ are the velocity components in the direction of coordinate vectors at a current point, and

$$\zeta_{11} = \left(\frac{\partial x}{\partial x_1}\right)^2 + \left(\frac{\partial y}{\partial x_1}\right)^2,$$
$$\zeta_{22} = \left(\frac{\partial x}{\partial x_2}\right)^2 + \left(\frac{\partial y}{\partial x_2}\right)^2,$$
$$\zeta = \zeta_{11} \cdot \zeta_{22}.$$

Thus the original system (1) written in scalar form for arbitrary orthogonal coordinates (x_1, x_2) becomes

$$\frac{\partial h}{\partial t} + \frac{1}{\sqrt{\zeta}} \cdot \frac{\partial}{\partial x_1}\left(hV_1\sqrt{\zeta_{22}}\right) + \frac{1}{\sqrt{\zeta}} \cdot \frac{\partial}{\partial x_2}\left(hV_2\sqrt{\zeta_{11}}\right) = 0 \tag{2a}$$

$$\frac{\partial V_1}{\partial t} + \frac{V_1}{\sqrt{\zeta_{11}}}\frac{\partial V_1}{\partial x_1} + \frac{V_2}{\sqrt{\zeta_{22}}}\frac{\partial V_1}{\partial x_2} + g\frac{1}{\sqrt{\zeta_{11}}}\frac{\partial h}{\partial x_1} = g\frac{1}{\sqrt{\zeta_{11}}}\frac{\partial d}{\partial x_1} \tag{2b}$$

$$\frac{\partial V_2}{\partial t} + \frac{V_1}{\sqrt{\zeta_{11}}}\frac{\partial V_2}{\partial x_1} + \frac{V_2}{\sqrt{\zeta_{22}}}\frac{\partial V_2}{\partial x_2} + g\frac{1}{\sqrt{\zeta_{22}}}\frac{\partial h}{\partial x_2} = g\frac{1}{\sqrt{\zeta_{22}}}\frac{\partial d}{\partial x_2}. \tag{2c}$$

1.2 Splitting

Following the same approach as in (Titov and Synolakis, 1998), the above system is split in two systems by setting either $\partial/\partial x_2 = 0$ or $\partial/\partial x_1 = 0$. Furthermore,

$$ds_1 = \sqrt{\left(\frac{\partial x}{\partial x_1} \cdot dx_1\right)^2 + \left(\frac{\partial y}{\partial x_1} \cdot dx_1\right)^2} = \sqrt{\zeta_{11}} \cdot dx_1 \tag{3}$$

is an elementary distance along a coordinate curve $x_2 = \text{const}$. Likewise,

$$ds_2 = \sqrt{\left(\frac{\partial x}{\partial x_2} \cdot dx_2\right)^2 + \left(\frac{\partial y}{\partial x_2} \cdot dx_2\right)^2} = \sqrt{\zeta_{22}} \cdot dx_2 \tag{4}$$

is a differential of a distance along a coordinate curve $x_1 = \text{const}$. In terms of the distances s_1 and s_2, the two systems yielded by splitting are:

$$\frac{\partial h}{\partial t} + \frac{\partial}{\partial s_1}(hV_1) + hV_1 \cdot \frac{1}{\sqrt{\zeta_{22}}} \cdot \frac{\partial}{\partial s_1}\sqrt{\zeta_{22}} = 0 \tag{5a}$$

$$\frac{\partial V_1}{\partial t} + V_1\frac{\partial V_1}{\partial s_1} + g\frac{\partial h}{\partial s_1} = g\frac{\partial d}{\partial s_1} \tag{5b}$$

$$\frac{\partial V_2}{\partial t} + V_1\frac{\partial V_2}{\partial s_1} = 0 \tag{5c}$$

and

$$\frac{\partial h}{\partial t}+\frac{\partial}{\partial s_2}\left(hV_2\right)+hV_2\cdot\frac{1}{\sqrt{\zeta_{11}}}\cdot\frac{\partial}{\partial s_2}\sqrt{\zeta_{11}}=0 \tag{6a}$$

$$\frac{\partial V_2}{\partial t}+V_2\frac{\partial V_2}{\partial s_2}+g\frac{\partial h}{\partial s_2}=g\frac{\partial d}{\partial s_2} \tag{6b}$$

$$\frac{\partial V_1}{\partial t}+V_2\frac{\partial V_1}{\partial s_2}=0. \tag{6c}$$

The MOST method is a numerical technique of solving system (2) by computing solutions for the next time step of the simplified systems (5) and (6) sequentially. Computations in (5) are done along curves $x_2 = \text{const}$. Computations in (6) are done along curves $x_1 = \text{const}$.

The first two equations in (5) (and in (6) analogically) can be rewritten in terms of Riemann invariants (Titov and Synolakis, 1998; Burwell *et al.*, 2007)

$$p=V_1+2\sqrt{gh},\quad q=V_1-2\sqrt{gh}$$

and eigenvalues $\lambda_{1,2}=V_1\pm\sqrt{gh}$ as

$$\frac{\partial p}{\partial t}+\lambda_1\frac{\partial p}{\partial s_1}=g\frac{\partial d}{\partial s_1}-\frac{p^2-q^2}{8\sqrt{\zeta_{22}}}\cdot\frac{\partial}{\partial s_1}\sqrt{\zeta_{22}} \tag{7a}$$

$$\frac{\partial q}{\partial t}+\lambda_2\frac{\partial q}{\partial s_1}=g\frac{\partial d}{\partial s_1}+\frac{p^2-q^2}{8\sqrt{\zeta_{22}}}\cdot\frac{\partial}{\partial s_1}\sqrt{\zeta_{22}}. \tag{7b}$$

Adding equations (7) together simplifies to (5b). Subtracting the two equations simplifies to (5a).

Similarly, the first two equations in (6) can be rewritten as:

$$\frac{\partial \tilde{p}}{\partial t}+\tilde{\lambda}_1\frac{\partial \tilde{p}}{\partial s_2}=g\frac{\partial d}{\partial s_2}-\frac{\tilde{p}^2-\tilde{q}^2}{8\sqrt{\zeta_{11}}}\cdot\frac{\partial}{\partial s_2}\sqrt{\zeta_{11}} \tag{8a}$$

$$\frac{\partial \tilde{q}}{\partial t}+\tilde{\lambda}_2\frac{\partial \tilde{q}}{\partial s_2}=g\frac{\partial d}{\partial s_2}+\frac{\tilde{p}^2-\tilde{q}^2}{8\sqrt{\zeta_{11}}}\cdot\frac{\partial}{\partial s_2}\sqrt{\zeta_{11}} \tag{8b}$$

where

$$\tilde{p}=V_2+2\sqrt{gh},\quad \tilde{q}=V_2-2\sqrt{gh},\quad \tilde{\lambda}_{1,2}=V_2\pm\sqrt{gh}.$$

1.3 Particular Case: MOST in Cartesian Coordinates

In Cartesian coordinates (x, y),

$$\frac{\partial}{\partial s_1}=\frac{\partial}{\partial x},\quad \frac{\partial}{\partial s_2}=\frac{\partial}{\partial y},\quad \zeta_{11}=\zeta_{22}=1.$$

The last term on the right side of the equations (5a), (6a), and the systems (7) and (8) equals zero.

1.4 Particular Case: MOST on Spherical Earth

Let R denote Earth's radius, θ be a latitude at an observation point, and ϕ be the point's longitude. (x, y) is the rectangular coordinate system in the horizontal plane with an origin at the observation point, with the x-axis pointing west to east and the y-axis pointing south to north. Then

$$dx = ds_1 = R\cos(\theta)d\phi, \quad dy = ds_2 = Rd\theta, \quad V_1 = V_\phi, \quad V_2 = V_\theta \tag{9}$$

and

$$\sqrt{\zeta_{11}} = R\cos(\theta), \quad \sqrt{\zeta_{22}} = R, \quad \frac{\partial}{\partial s_1} = \frac{1}{R\cos(\theta)} \cdot \frac{\partial}{\partial \phi}, \quad \frac{\partial}{\partial s_2} = \frac{1}{R} \cdot \frac{\partial}{\partial \theta}. \tag{10}$$

Systems (5) and (6), (7) and (8) turn into those solved currently in MOST (Titov and González, 1997), with the last term being zero when calculations are done west to east, and the last term being

$$\frac{1}{\sqrt{\zeta_{11}}} \cdot \frac{\partial}{\partial s_2}\sqrt{\zeta_{11}} = \frac{1}{R\cos(\theta)} \cdot \frac{1}{R} \cdot \frac{\partial}{\partial \theta}\left(R\cos(\theta)\right) = -\frac{1}{R}\tan(\theta) \tag{11}$$

when calculations are done along a meridian.

2. Curvilinear MOST: The Code

2.1 MOST Code Versions

MOST code version 4, presented below and referred to as curvilinear MOST, continues the previous code development known inside NCTR as MOST versions 1 to 3. Below is a brief overview of MOST version features as the code was gradually transformed toward greater generality and functionality:

- Version 1: computations in spherical coordinates (longitude, latitude) in grids A and B, run-up on land in grid C. The run-up routine does not account for metric factors due to spherical geometry, so a grid C (only a few to tens of kilometers in extent) is actually treated as flat. Since neither drying of initially wet cells nor wetting of initially dry cells is allowed in grids A and B, reflective boundary conditions are imposed at a depth of 10–20 m in these grids. Grids A and B have an outer boundary (with the database grid or a grid A, accordingly) and an inner boundary (with a grid B or C, accordingly). The grids provide boundary inputs for each other. The difference scheme is written in terms of the distances between grid nodes, and allows for non-uniform spacing in either coordinate direction (Titov and Synolakis, 1998).

- Version 2 (the current operational version in NCTR): the cell's wetting/drying interface is implemented in spherical coordinates in grids A and B. The boundary with an inner grid (and consequently, the input from the inner grid) is removed. The computations in grids A

and B are carried all the way to the shore (up to 1 m depth) and are independent of computations in the enclosed grid. Three different routines are used in version 2 for advancing the solution one time step forward according to 1D systems (5) and (6) and computing run-up: SWRUN_LON and SWRUN_LAT (used in grids A and B for computations in meridional and zonal directions, accordingly), and SWRUN (used in grid C for both directions).

- Version 3: the version 2 code has been clarified and unified. In particular, the metric factors were gathered together in a separate section of the code. As a result, one routine, DSWRUN, replaced the three above, with an additional argument to select the metric factors for the zonal or meridional direction (or for the flat surface, if needed). Grid C is not considered flat anymore. All the grids are given individual flags to select among the three run-up options: (1) reflecting wall near the beach with no cell's drying, (2) reflecting wall with cell's drying (run-down), or (3) run-up on the beach. The general organization of the code was changed to allow for an arbitrary number and configuration of grids (Chawla *et al.*, 2008). As in version 2, an outer grid provides an input to an inner grid but does not receive any feedback and runs independently of the enclosed grids. As in the first version, all the older versions can handle uneven spacing in the zonal and/or meridional direction.

The original first version of the MOST code was developed by Dr. V. Titov in 1989–1997. Versions 2 and 3 were developed in 2005–2006 by Dr. A. Chawla and Dr. D. Burwell.

In versions 1–3, all the MOST grids are rectangles in a longitude/latitude plane, bounded by two parallels and two meridians. Some research varieties of versions 2/3 can process data in Cartesian coordinates. In light of the previous code development, rather straightforward changes are needed to enable MOST version 3 to process data sampled on an arbitrary curvilinear grid. The changes were/are to be made:

- to the difference scheme;
- to the bathymetry format;
- to the handling of the boundary input from the database;
- to the handling of the input from an outer grid into inner ones—not yet implemented.

These changes, detailed below, resulted in MOST version 4 (implemented in Fortran 95), which can process data fields in an arbitrary orthogonal curvilinear coordinate system.

2.2 Metric Factors in the Difference Scheme

The above-mentioned DSWRUN routine can be used with rows and columns of a $M \times N$ grid in arbitrary orthogonal curvilinear coordinates, if row/column

spacings and geometry-dependent last terms in systems (7) or (8) are provided as the routine arguments. The next four matrices represent metric factors provided as an input for DSWRUN in the curvilinear MOST:

- $(M-1)\times N$ matrix $s1$, whose columns are the distances between neighboring nodes in the data field columns;

- $(N-1)\times M$ matrix $s2$, whose columns are the distances between neighboring nodes in the data field rows;

- $M\times N$ matrix $g22s1$ of scaling factors

$$g22s1=\frac{1}{\sqrt{\zeta_{22}}}\cdot\frac{\partial}{\partial s_1}\sqrt{\zeta_{22}}=\frac{dx_2}{ds_2}\cdot\frac{\partial}{\partial s_1}\frac{ds_2}{dx_2}\ . \tag{12}$$

  Let Δs_2 be the distance between coordinate curves $x_2=c$ and $x_2=c+\Delta x_2$ associated with neighboring data columns. Δs_2 varies with x_1 along the curves, while Δx_2 is fixed. Therefore

$$g22s1\approx\frac{1}{\Delta s_2}\cdot\frac{\partial}{\partial s_1}\Delta s_2\ . \tag{13}$$

  The distances from the (i,j) element of the data to the neighboring nodes are shown in Fig. 2-1. Using centered differences (except for the elements in the first and last row) for the first derivative with respect to s_1 and averaging the results (except for the first and last columns) left and right on the current node yields

$$\begin{aligned}g22s1(i,j)=\frac{1}{2}\frac{1}{s2(j,i)}\frac{s2(j,i+1)-s2(j,i-1)}{s1(i-1,j)+s1(i,j)}+\\+\frac{1}{2}\frac{1}{s2(j-1,i)}\frac{s2(j-1,i+1)-s2(j-1,i-1)}{s1(i-1,j)+s1(i,j)}\ .\end{aligned} \tag{14}$$

  To calculate the elements of the first/last column of the matrix $g22s1$, only the first/last term in (14) is used, without the factor 1/2. The elements of the first/last row are calculated as

$$\begin{aligned}g22s1(1,j)&=\frac{1}{s2(j,1)}\frac{s2(j,2)-s2(j,1)}{s1(1,j)},\\ g22s1(M,j)&=\frac{1}{s2(j,M)}\frac{s2(j,M)-s2(j,M-1)}{s1(M-1,j)}\ .\end{aligned} \tag{15}$$

- Similarly, $N\times M$ matrix $g11s2$ of scaling factors

$$\frac{1}{\sqrt{\zeta_{11}}}\cdot\frac{\partial}{\partial s_2}\sqrt{\zeta_{11}}\approx\frac{1}{\Delta s_1}\cdot\frac{\partial}{\partial s_2}\Delta s_1\ , \tag{16}$$

  where Δs_1 is the distance between coordinate curves $x_1=c$ and $x_1=c+\Delta x_1$ (data rows), varying with x_2, calculated (except for the first

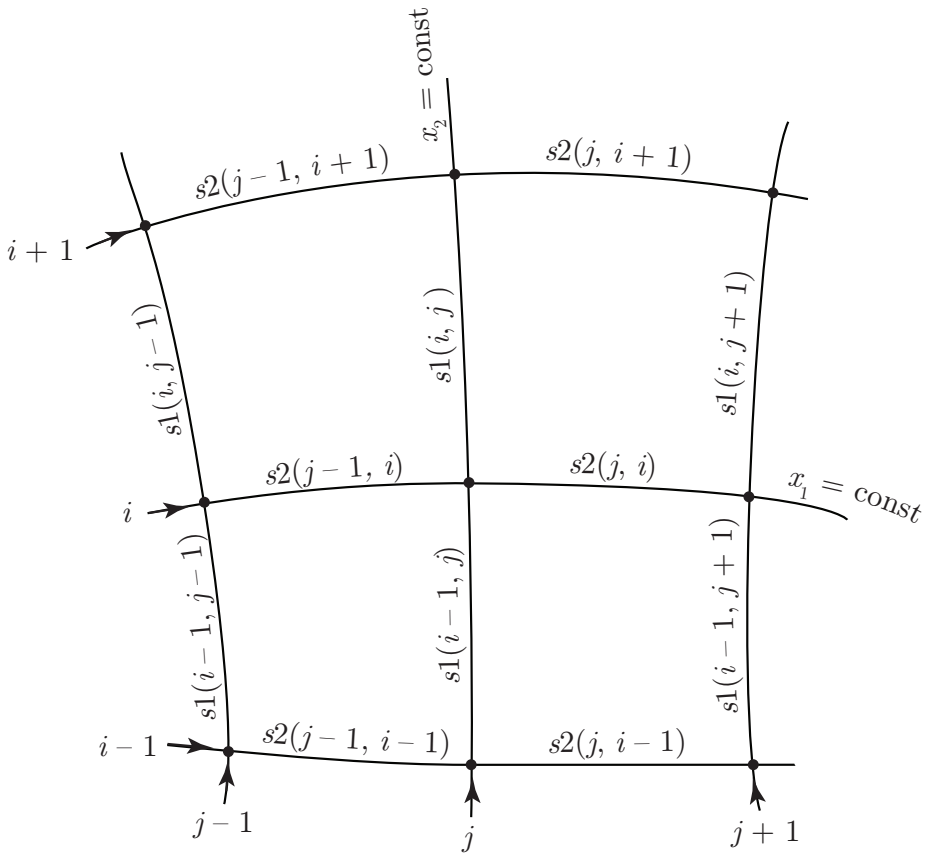

Figure 2-1: The distances from the (i, j) grid element to the neighboring nodes.

and last rows and columns, where the difference scheme has to include fewer elements) as:

$$g11s2(j,i) = \frac{1}{2}\frac{1}{s1(i,j)}\frac{s1(i,j+1)-s1(i,j-1)}{s2(j-1,i)+s2(j,i)} + \tag{17}$$

$$+\frac{1}{2}\frac{1}{s1(i-1,j)}\frac{s1(i-1,j+1)-s1(i-1,j-1)}{s2(j-1,i)+s2(j,i)}\,.$$

As mentioned above, MOST reduces the 2-D problem to a series of 1-D problems. In the MOST numerical implementation (version 3 and older), the DSWRUN routine is performed over each row of the data field, according to equations (7) and (5c), and then over each column according to equations (8) and (6c), thus advancing the solution one time step forward. For the curvilinear version, when computations are run over the j-th column of the data, DSWRUN needs to use the j-th column of each matrix $s1$ and $g22s1$. When computations are run over the i-th row of the data, DSWRUN needs to use the i-th column of each matrix $s2$ and $g11s2$.

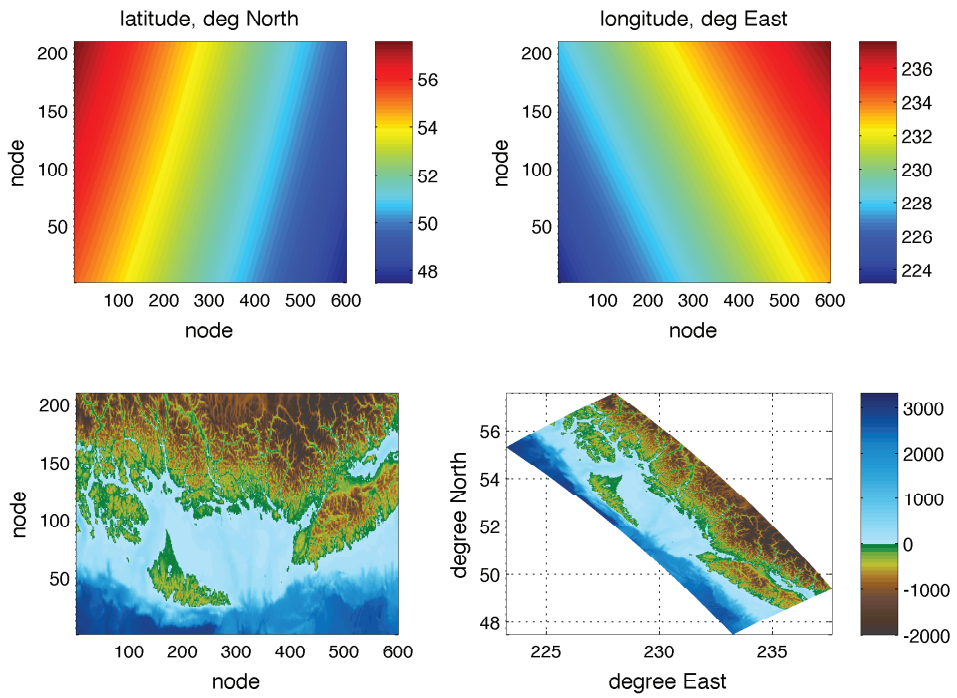

Figure 2-2: Latitude, longitude, and bathymetry matrices, and the same area in longitude/latitude axes.

2.3 Bathymetry Format for a Curvilinear Grid on the Globe

In versions 1–3, all the MOST data fields (surface elevation at a given time, instant velocities, undisturbed water depth (bathymetry)) are $M \times N$ matrices positioned on the grids in a longitude/latitude reference frame. A grid is given by the N-element vector of its nodes' longitudes and the M-element vector of its nodes' latitudes. In the curvilinear version intended for computations on the globe, both the data fields and the grid nodes' longitudes and latitudes are $M \times N$ matrices whose (i, j) element has coordinates $(x_1(i), x_2(j))$ in some reference frame. As an example, Fig. 2-2 shows longitude, latitude, and bathymetry matrices for some area in some coordinate system as they would be present in computations, and the same area in the longitude/latitude axes.

Given the arrays of the nodes' longitudes $h1$ and latitudes $h2$ (in decimal degrees), the matrix of metric factors $s1$ (and similarly, $s2$) can be calculated as

$$s1(i,j) = 111320 \cdot \left(\Delta x^2 + \Delta y^2\right)^{1/2}, \tag{18}$$

where 111320 is a length of 1 arc-degree of the Earth meridian in meters, and

$$\Delta x = (h1(i+1,j) - h1(i,j)) \cdot cos\frac{\pi}{360}\left(h2(i,j) + h2(i+1,j)\right), \tag{19a}$$

$$\Delta y = h2(i+1,j) - h2(i,j). \tag{19b}$$

2.4 Database Input Through the Boundaries

In a typical MOST application scenario, a wave enters a computational domain through the grid boundary. It is given by surface elevation and two velocity fields, pre-calculated on an ocean-wide coarse grid in the longitude/latitude frame (Gica *et al.*, 2008), also referred to as a source grid. Two boundary values for water elevation and two velocity components normal and tangent to the grid boundary, interpolated from the source grid onto the boundary of the computational domain, are yet another six arguments requested by DSWRUN. The source velocities, however, are west-to-east current and south-to-north current, and therefore have to be projected onto directions of the grid lines at each node on the grid boundary.

Let (i,j) be a point P on the grid boundary at latitude angle (in radians) $\theta = \pi \cdot h1(i,j)/180$, and let u and v be zonal and meridional currents at this point. The velocity vector can then be written as

$$\vec{V} = u \cdot \vec{z} + v \cdot \vec{m}, \tag{20}$$

where $\vec{z}$ and $\vec{m}$ are zonal and meridional unit vectors at point P.

Let $(i+\Delta i, j+\Delta j)$ be the grid inner point P_1, closest to the given boundary point $P(i,j)$. The direction given by the two points P and P_1 is then orthogonal to the boundary. Possible values for the indexes are:

- $j = 1, \quad \Delta i = 0, \quad \Delta j = 1$ for the boundary associated with the first column of the data;
- $j = N, \quad \Delta i = 0, \quad \Delta j = -1$ for the last column;
- $i = 1, \quad \Delta i = 1, \quad \Delta j = 0$ for the first row;
- $i = M, \quad \Delta i = -1, \quad \Delta j = 0$ for the last row.

A unit vector $\vec{n}(i,j)$ orthogonal to the boundary at point P can be found as

$$\vec{n} = a_n \cdot \vec{z} + b_n \cdot \vec{m}, \tag{21}$$

where

$$a_n = cos(\theta)\Delta\phi / \sqrt{(cos(\theta)\Delta\phi)^2 + \Delta\theta^2}, \tag{22a}$$

$$b_n = \Delta\theta / \sqrt{(cos(\theta)\Delta\phi)^2 + \Delta\theta^2}; \tag{22b}$$

$\Delta\theta$ and $\Delta\phi$ are the increases in latitude and longitude between points P and P_1. A unit vector tangent to the boundary at a current point P can be found as

$$\vec{\tau}(i,j) = \pm(-b_n \cdot \vec{z} + a_n \cdot \vec{m}), \tag{23}$$

where the $\pm$ sign is selected so the vector $\vec{\tau}$ points in the positive direction of the grid line.

Then the velocity components normal and tangent to the grid boundary at a point (i, j) can be found as

$$V_n = a_n u + b_n v \tag{24a}$$

$$V_\tau = \pm(-b_n u + a_n v). \tag{24b}$$

3. Regional Forecast Version 2, West Coast

The first test for the Curvilinear MOST described here is the Regional Forecast version 2 that employs elongated curvilinear grids oriented along a coastline. Figure 2-3 shows three grids of the Regional Forecast version 2, numbered south to north and referred to as grid 1/2/3. The three grids cover almost as much of the coast as ten grids of Regional Forecast version 1, that is, all the West Coast from the tropic of Cancer and up to Alaska. The grids' ocean-side boundary is drawn at 2500 m depth or deeper, where the database provides valid input. The grids' resolution everywhere is 1 arc-min, found to be the optimal resolution for maximum wave height estimate purposes (see the chapter on Regional Forecast version 1). The grids' size is, respectively, 150 $\times$ 960, 196 $\times$ 720, and 210 $\times$ 600 nodes. In each grid, 10 hours of simulation starting with the moment when a wave enters the grid takes about 5 min to run, which reduces by several times the computational expenses for forecasting the wave height coast-wide, compared with version 1 (a Portland Group compiler with optimization capabilities and a rather powerful computer (Dell PowerEdge Linux machine, 2 $\times$ 3.6 GHz CPUs) were used for both versions).

Another feature of version 2 is that with grid columns oriented roughly normal to the coast and the assumption that a wave grows toward the coast, the maximum wave height at every column at every instant can serve as an estimate for an instant amplitude of the wave motion near the shore. Figure 2-4 shows a snapshot of a possible output of the Regional Forecast. The maximum wave heights in every column in the three grids are plotted against the distance in km from a grid's northern edge along a grid's longer side (with 1 arc-min spacing, the distance is 1.86 km multiplied by a column's number minus one) in the same axes every one or few timesteps. The previous output was overlaid in gray, before the current output was plotted in black. Thus the output presents the instant intensity of the wave motion near the shore, and at the same time records any previous maximum amplitude. The tsunami example simulated here is the 11/15/2006 tsunami, generated by an earthquake near the Kuril Islands. It arrived at the West Coast several cm high, with up to 0.5 m waves at places such as Crescent City and Santa Barbara.

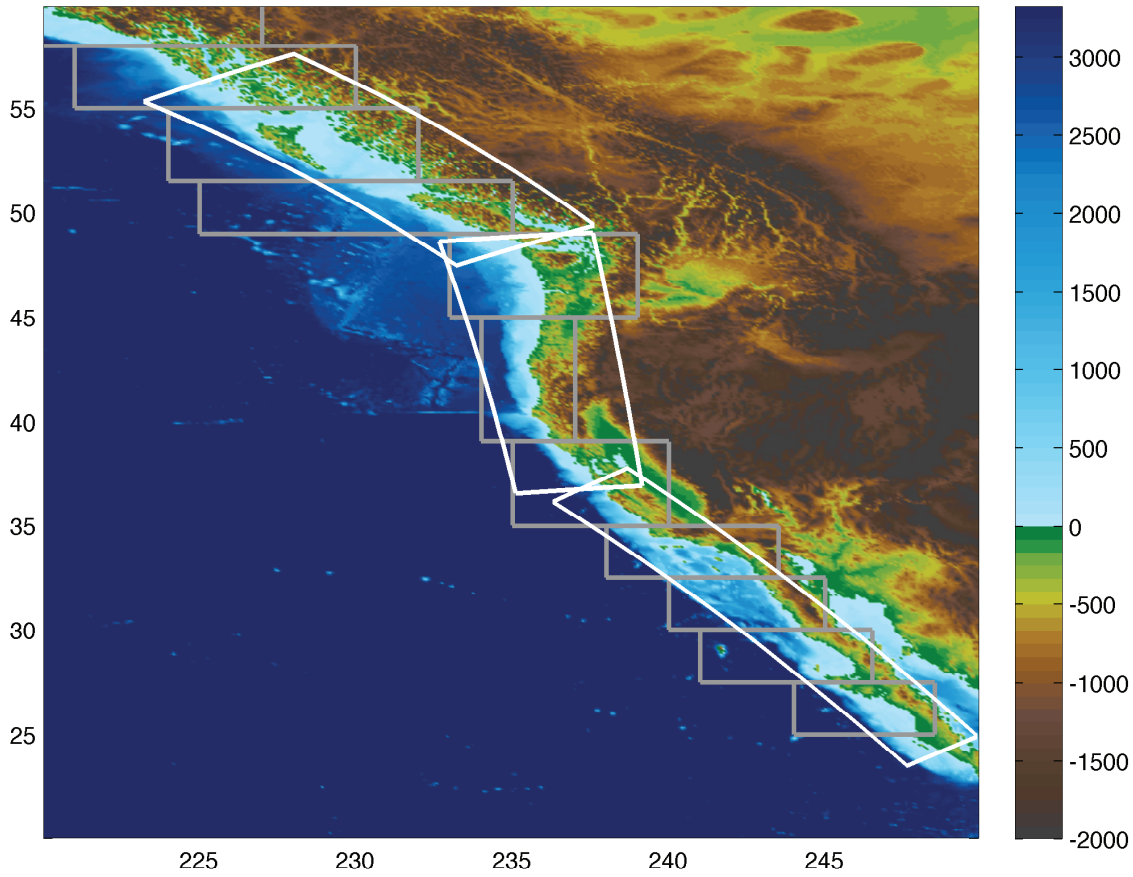

Figure 2-3: Grids 10–20 of Regional Forecast v.1 (gray, numbered north to south) and grids 1–3 of Regional Forecast v.2 (white, numbered south to north). Axes: longitude (°E), latitude (°N).

3.1 Shoreline-Oriented Grids for Regional Forecast

On the surface of the globe, the shoreline-oriented grids have cells shaped as almost perfect squares. The grids were cut in a spherical coordinate system, with ϑ for a zenith and φ for an azimuth angle, associated with a rectangular coordinate system $\tilde{K}$ with an origin at the Earth center O. The $\tilde{K}$ system is positioned so that a grid's ocean-side boundary falls on an "equator" in $\tilde{K}$, that is, a great circle in the plane $\tilde{z} = 0$. Longitude and latitude are associated with a rectangular coordinate system K with an origin in O, the z-axis pointing south to north, and the x-axis pointing to the Prime meridian.

The back and forth transformation between the systems K and $\tilde{K}$ can be developed in the following steps (see Fig. 2-5):

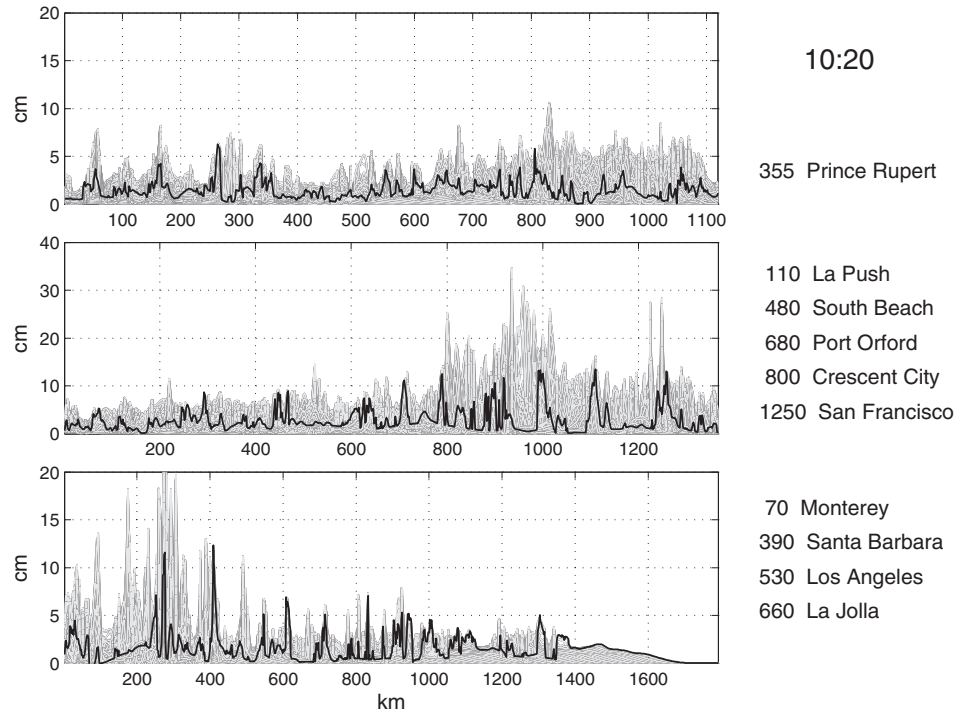

Figure 2-4: Coastline wave height estimate in grids 3-1 (top to bottom) vs. distance from the grid's northern edge. The distances for a number of sites are listed on the right. Black: near-shore amplitude at 10:20 since the quake; gray—amplitudes that occurred prior to 10:20. The wave has not yet reached the southern edge of grid 1.

- Turn the system K with respect to the z-axis through an angle α found as

$$\begin{Vmatrix} x_A & y_A & z_A \\ x_B & y_B & z_B \\ cos(\alpha) & sin(\alpha) & 0 \end{Vmatrix} = 0, \tag{25}$$

  where (x_A, y_A, z_A) and (x_B, y_B, z_B) are the coordinates of the two points A and B in K, computed given the points' longitudes and latitudes. The two points define a grid's ocean side boundary. The first rotation matrix

$$M_z = \begin{pmatrix} cos(\alpha) & -sin(\alpha) & 0 \\ sin(\alpha) & cos(\alpha) & 0 \\ 0 & 0 & 1 \end{pmatrix} \tag{26}$$

  transforms (x, y, z) coordinates to $(\tilde{x}, y_1, z)$ coordinates, with the $\tilde{x}$ axis on the intersection of the equatorial plane and the great circle containing the points A and B.

- Turn the coordinate axes $(\tilde{x}, y_1, z)$ with respect to the $\tilde{x}$-axis through an angle β from the positive z-axis to a great circle containing points

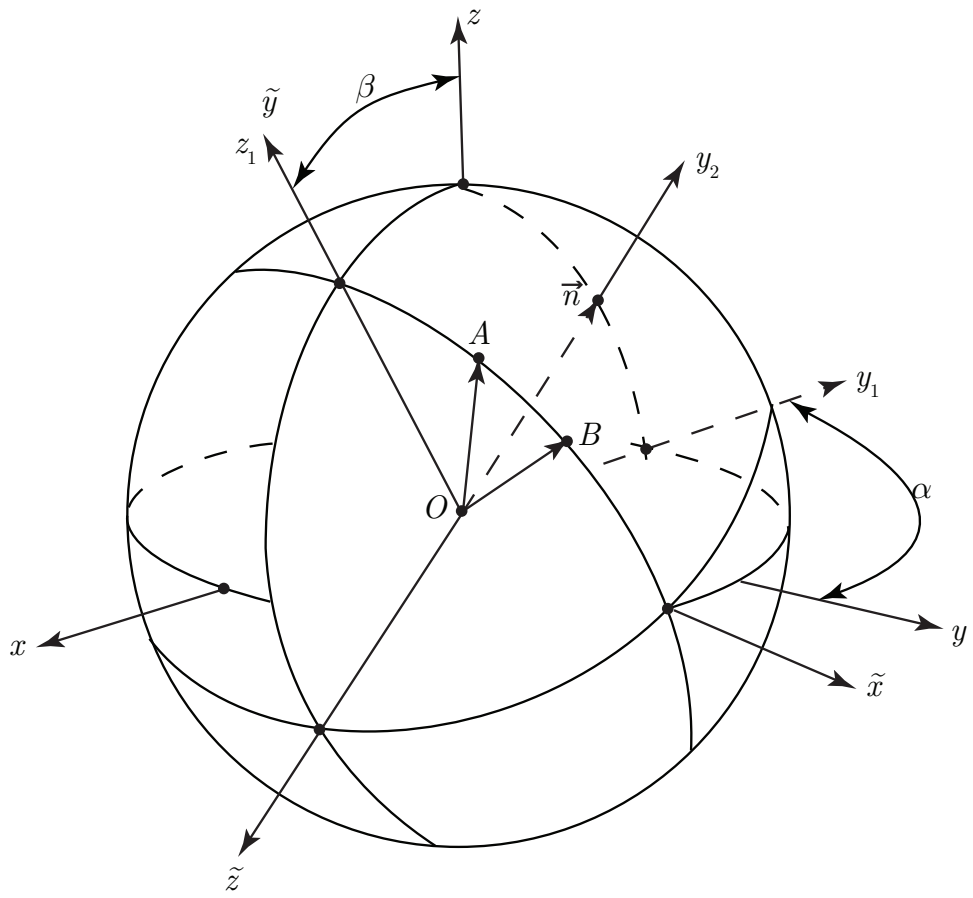

Figure 2-5: The transformation from K to $\tilde{K}$ coordinate system.

A and B. The angle β can be found as $\pm\arcsin(n_z)$, where n_z is a z-component in K of a unit vector $\vec{n}$ orthogonal to the great circle:

$$\vec{n} = \frac{\overrightarrow{OA} \times \overrightarrow{OB}}{||\overrightarrow{OA} \times \overrightarrow{OB}||} \,. \tag{27}$$

The second rotation matrix

$$M_x = \begin{pmatrix} 1 & 0 & 0 \\ 0 & cos(\beta) & -sin(\beta) \\ 0 & sin(\beta) & cos(\beta) \end{pmatrix} \tag{28}$$

transforms $(\tilde{x}, y_1, z)$ coordinates to $(\tilde{x}, y_2, z_1)$ coordinates, with $\tilde{x}$ and z_1 axes being in the great circle containing points A and B.

- The third rotation with respect to the $\tilde{x}$-axis through the right angle, associated with the rotation matrix

$$M_{xx} = \begin{pmatrix} 1 & 0 & 0 \\ 0 & 0 & 1 \\ 0 & -1 & 0 \end{pmatrix}, \tag{29}$$

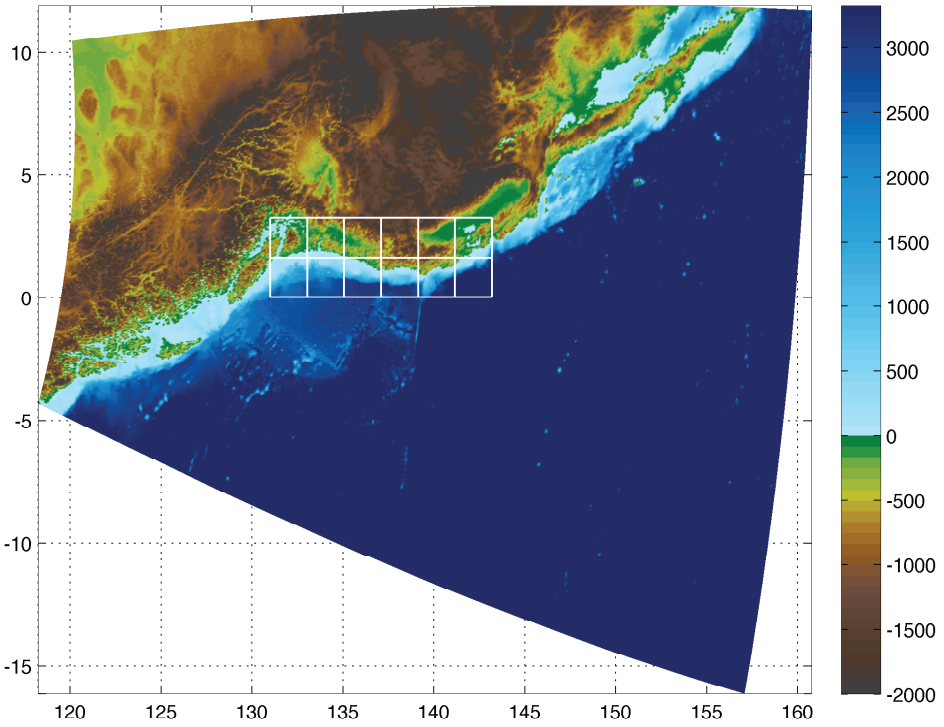

Figure 2-6: The map and grid 2 in (φ, ϑ) axes (in degrees).

completes the transformation by moving the y_2-axis into the great circle and the z_1-axis orthogonal to it.

Figure 2-6 shows the map and grid 2, presented in Fig. 2-3, in (φ, ϑ) axes used to develop the grid (zenith angle ϑ is counted from an orthogonal projection of a radius-vector in the $\tilde{x}$-$\tilde{y}$ plane to the vector, and represents latitude in the $\tilde{K}$ system). After the grid nodes were assigned at desired intervals in (φ, ϑ) coordinates, they were re-calculated in $(\tilde{x}, \tilde{y}, \tilde{z})$ coordinates and then transformed to (x, y, z) coordinates as

$$\begin{pmatrix} x \\ y \\ z \end{pmatrix} = M_z^T \cdot M_x^T \cdot M_{xx}^T \cdot \begin{pmatrix} \tilde{x} \\ \tilde{y} \\ \tilde{z} \end{pmatrix}. \tag{30}$$

Given the nodes' positions on the globe in the K system, their longitudes, latitudes, and corresponding bathymetry values can be found.

3.2 Differences Between the Regional Forecast Versions' Computation Results

Figures 2-8–2-10 display a comparison between the results of the modeling of the 11/15/2006 tsunami using the two versions of the Regional Forecast. For a number of sites along the coast, a time series calculated by v.1 (cyan)

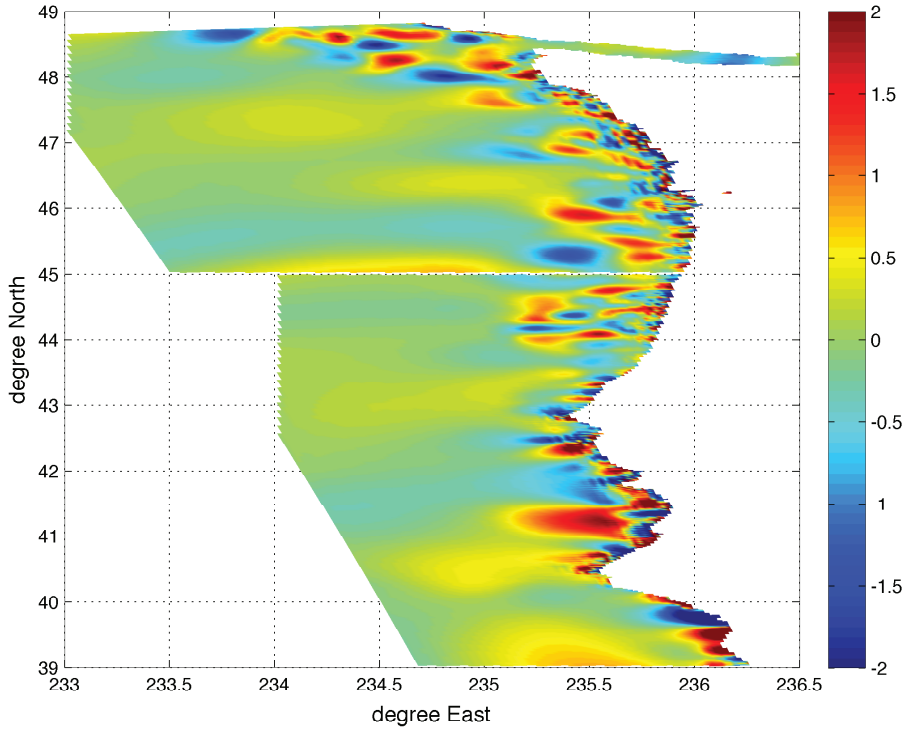

Figure 2-7: A snapshot of the difference between the wave fields in grids 14–15 and in the same area in grid 2. Colorbar: cm.

and a time series calculated by v.2 (black) are shown. The first wave or waves of the two time series at each site match perfectly. Later waves match in general.

Figure 2-7 shows a typical snapshot of the difference between the wave fields computed in grids 14 and 15, and in the same area in grid 2. The difference between the two solutions propagates from the boundaries between the smaller grids, and is due to the differences in the input into the area enclosed by a smaller grid. In version 1, the input into each small grid area comes from the database on each of three sides (the remaining 4th side is land). In version 2, the input into the area comes from the database on the ocean side, and from neighboring areas of the longer grid on the other two sides. Input from the database is the only way the smaller grids of version 1 can account for the waves traveling along the coast. In coastal waters, however, the database solution is too approximate. Longer grids of version 2 are therefore expected to provide a more accurate estimate for the wave component propagating in the longshore direction.

Nothing in the difference field comes from the ocean side, thus indicating that in deep water the database solution is accurate and therefore the Regional Forecast solution does not depend on the exact position of the grid boundary in deep water.

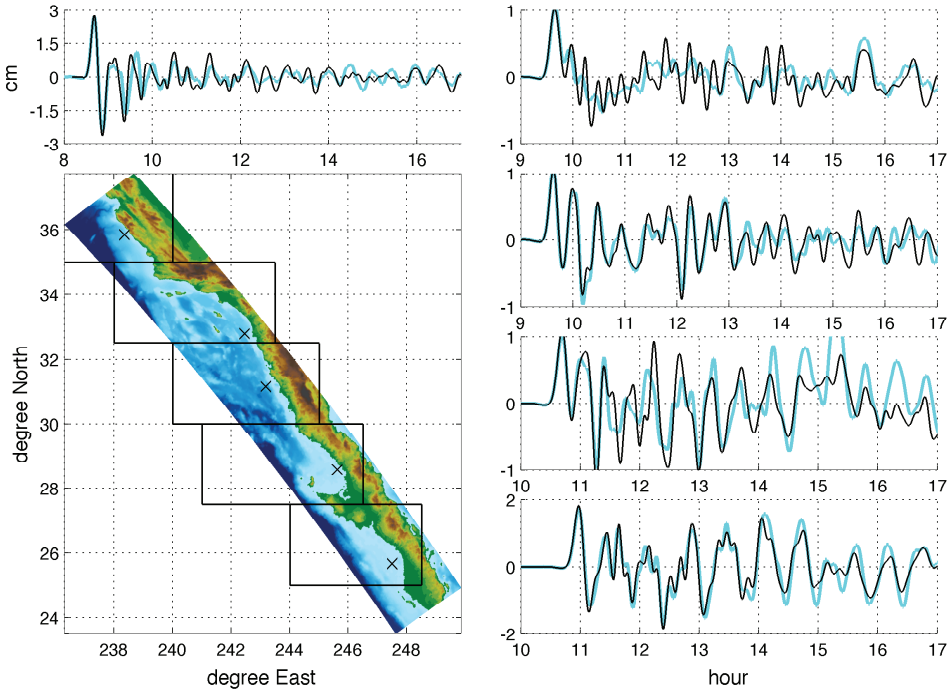

Figure 2-8: Time series in observation points (crosses in the map) of the 11/15/2006 tsunami, calculated in grid 1 of Regional Forecast version 2 (black/thin) and in grids 16–20 of Regional Forecast version 1 (cyan/thick).

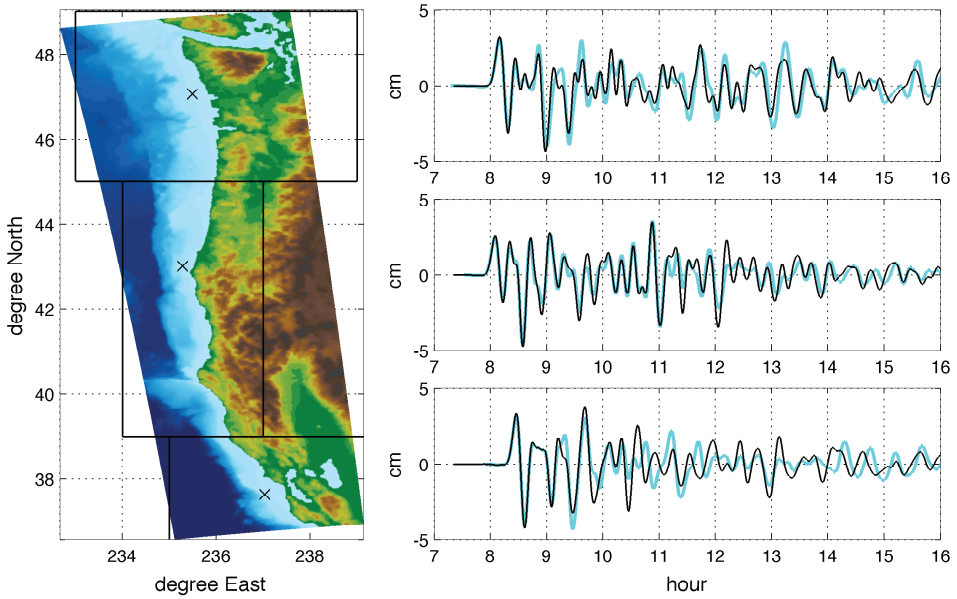

Figure 2-9: Time series in observation points (crosses in the map) of the 11/15/2006 tsunami, calculated in grid 2 of Regional Forecast version 2 (black/thin) and in grids 14–16 of Regional Forecast version 1 (cyan/thick).

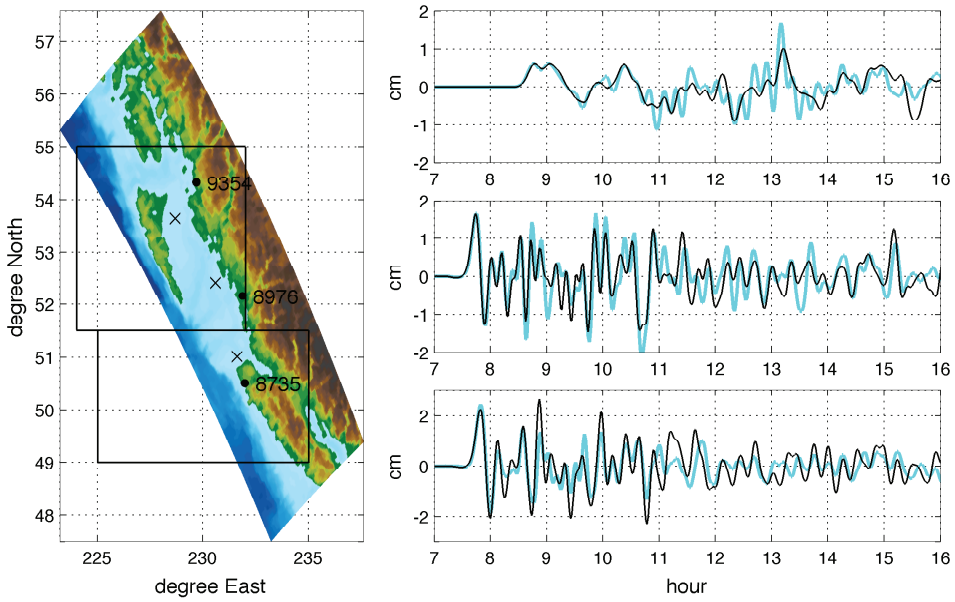

Figure 2-10: Time series in three observation points (crosses in the map) of the 11/15/2006 tsunami, calculated in grid 3 of Regional Forecast version 2 (black/thin) and in grids 12 and 13 of Regional Forecast version 1 (cyan/thick). Black dots: locations of the tide gages (9354—Prince Rupert, 8976—Bella Bella, 8735—Winter Harbor, BC).

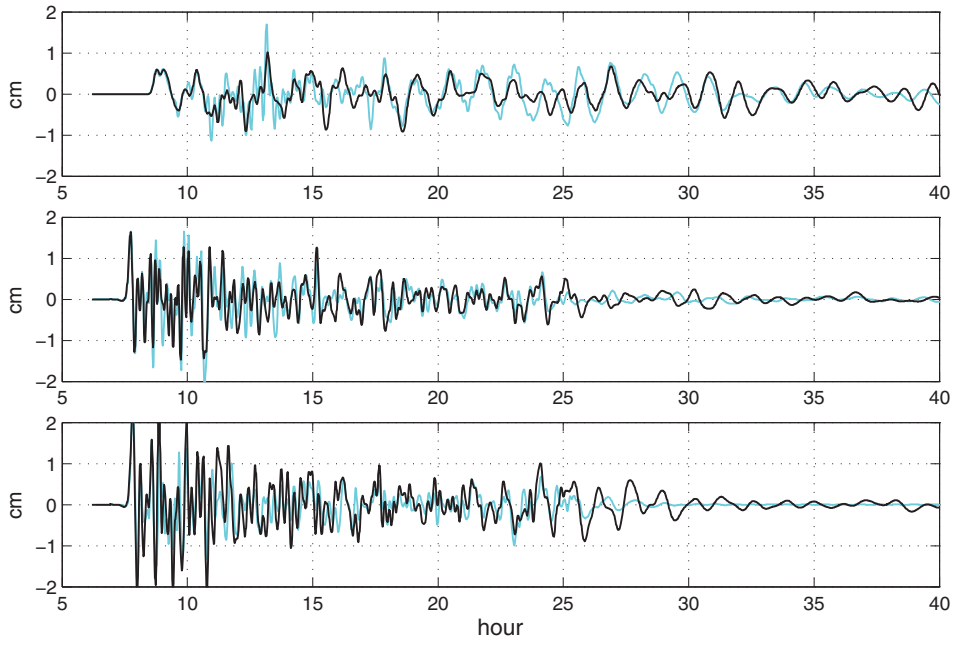

Figure 2-11: Grid 3 vs. 12–13, same observation points, longer time series.

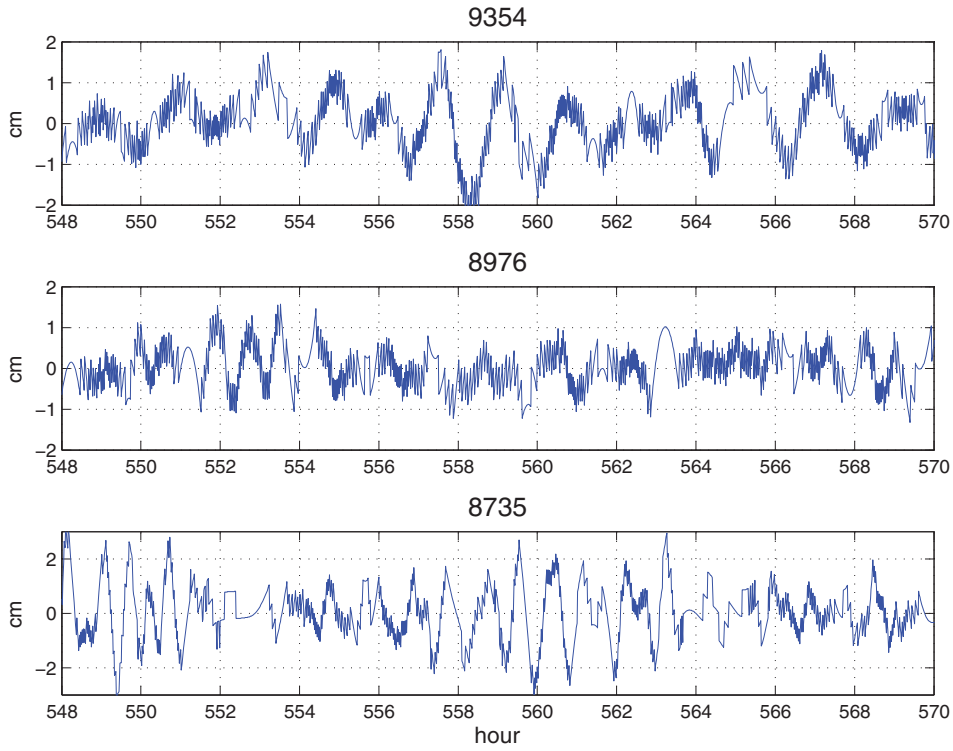

Figure 2-12: Examples of de-tided tide gage records in the area under ordinary conditions.

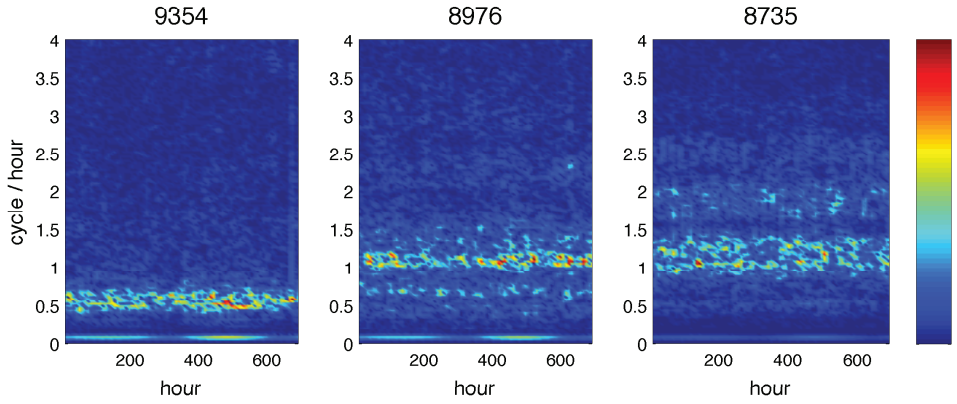

Figure 2-13: Spectrograms of the gage records (taken 08/2005).

The most significant difference between the solutions of the two versions occurs in the area enclosed by Queen Charlotte Island, Vancouver Island, and the mainland (grid 3). The area is a natural resonator. Records at the local tide gages display ever-present oscillations (Fig. 2-12). Figure 2-13 shows the spectrograms (amplitude of the Short Time Fourier Transform (STFT)) of the gages' records. Each gage record was 1 month long, sampled at 1-min intervals. STFT was computed over 2048-min-long sections of the record, weighted using a Hamming window, with 512 min $\approx$ 8.5 hour shift between the sections. There are clear spectral lines indicating ever-present oscillations at a period about 1 hour for 8976 and 8735, or 2 hours for 9354.

Modeled time series (Fig. 2-11) also reveal the area's resonating properties. The time series start at the higher (tsunami) frequency, but continue at a longer period of about 1.2 hour. A little of the direct tsunami wave reaches the most northern observation point, so the corresponding time series start with the lower (resonator) frequency (Fig. 2-11, top pane). Still, the version 1 solution (cyan) shows a more intensive component at the tsunami frequency than the version 2 solution (black), since in version 1 the tsunami was introduced directly inside the resonator through the southern boundary of grid 12. The wave motion remains in the version 2 solution for hours after the database input had stopped at the 24-hour marker. In the version 1 solution, the area calms down faster, since the wave energy leaves the resonator through the southern boundary of grid 12/northern boundary of grid 13.

Otherwise, the solutions by the two versions are in good agreement, which increases our confidence in both.

4. Acknowledgments

This study and publication are funded by NOAA and by the Joint Institute for the Study of the Atmosphere and Ocean (JISAO) under NOAA Cooperative Agreement No. NA17RJ1232, Contribution # 1595 (JISAO) and # 3231 (PMEL).

Sincere thanks are due to Ryan L. Whitney for proofreading and editing the manuscript.

References

Burwell, D., E. Tolkova, and A. Chawla (2007): Diffusion and dispersion characterization of a numerical tsunami model. *Ocean Modelling*, *19*(1–2), 10–30.

Chawla, A., J. Borrero, and V. Titov (2008): Evaluating wave propagation and inundation characteristics of the MOST tsunami model over a complex 3D beach. To appear in a Proceedings Volume for the Long-Wave Runup Workshop, 261–267.

Gica, E., M.C. Spillane, V.V. Titov, C.D. Chamberlin, and J.C. Newman (2008): Development of the forecast propagation database for NOAA's Short-Term Inundation Forecast for Tsunamis (SIFT). NOAA Technical Memorandum OAR PMEL-139, NOAA/Pacific Marine Environmental Laboratory, Seattle, WA, 89 pp.

Tang, L., C. Chamberlin, E. Tolkova, M. Spillane, V.V. Titov, E.N. Bernard, and H.O. Mofjeld (2006): Assessment of potential tsunami impact for Pearl Habor, Hawaii. NOAA Technical Memorandum OAR PMEL-131, NOAA/Pacific Marine Environmental Laboratory, Seattle, WA, 36 pp.

Titov, V.V., and F.I. González (1997): Implementation and testing of the Method of Splitting Tsunami (MOST) model. NOAA Technical Memorandum ERL PMEL-112, NOAA/Pacific Marine Environmental Laboratory, Seattle, WA, 11 pp.

Titov, V.V., F.I. González, E.N. Bernard, M.C. Eble, H.O. Mofjeld, J.C. Newman, and A.J. Venturato (2005): Real-time tsunami forecasting: Challenges and solutions. *Nat. Hazards*, *35*(1), Special Issue, U.S. National Tsunami Hazard Mitigation Program, 41–58.

Titov, V.V., and C.S. Synolakis (1995): Modeling of breaking and nonbreaking long-wave evolution and runup using VTCS-2. *J. Waterw. Port Coast. Ocean Eng.*, *121*(6), 308–316.

Titov, V.V., and C.S. Synolakis (1998): Numerical modeling of tidal wave runup. *J. Waterw. Port Coast. Ocean Eng.*, *124*(4), 157–171.

Wei, Y., E. Bernard, L. Tang, R. Weiss, V. Titov, C. Moore, M. Spillane, M. Hopkins, and U. Kânoğlu (2008): Real-time experimental forecast of the Peruvian tsunami of August 2007 for U.S. coastlines. *Geophys. Res. Lett.*, *35,* L04609, doi: 10.1029/2007GL032250.

Yanenko, N.N. (1971): *The Method of Fractional Steps*. Springer, New York, Berlin, Heidelberg, translated from Russian by M. Holt.